Missouri State University

BearWorks

Articles by College of Natural and Applied Sciences Faculty

2014

Analysis of the rich frequency spectrum of KIC 10670103 revealing the most slowly rotating subdwarf B star in the Kepler field

Michael D. Reed
Missouri State University

Heather M. Foster
MSU Undergraduate

J H. Telting

R H. Østensen

L H. Farris
MSU Undergraduate

See next page for additional authors

Follow this and additional works at: https://bearworks.missouristate.edu/articles-cnas

Recommended Citation

Reed, Michael D., H. Foster, J. H. Telting, R. H. Østensen, L. H. Farris, R. Oreiro, and Andrzej S. Baran. "Analysis of the rich frequency spectrum of KIC 10670103 revealing the most slowly rotating subdwarf B star in the Kepler field." Monthly Notices of the Royal Astronomical Society 440, no. 4 (2014): 3809-3824.

This article or document was made available through BearWorks, the institutional repository of Missouri State University. The work contained in it may be protected by copyright and require permission of the copyright holder for reuse or redistribution.
For more information, please contact BearWorks@library.missouristate.edu.

Authors
Michael D. Reed, Heather M. Foster, J H. Telting, R H. Østensen, L H. Farris, R. Oreiro, and Andrzej Baran

This article is available at BearWorks: https://bearworks.missouristate.edu/articles-cnas/817

Monthly Notices
of the
ROYAL ASTRONOMICAL SOCIETY
MNRAS **440,** 3809–3824 (2014) doi:10.1093/mnras/stu412

Analysis of the rich frequency spectrum of KIC 10670103 revealing the most slowly rotating subdwarf B star in the *Kepler* field

M. D. Reed,[1]★ H. Foster,[1] J. H. Telting,[2] R. H. Østensen,[3] L. H. Farris,[1] R. Oreiro[4,5] and A. S. Baran[1,6]

[1]*Department of Physics, Astronomy and Materials Science, Missouri State University, 901 S. National, Springfield, MO 65897, USA*
[2]*Nordic Optical Telescope, Rambla José Ana Fernández Pérez 7, E-38711 Breña Baja, Spain*
[3]*Instituut voor Sterrenkunde, KU Leuven, Celestijnenlaan 200 D, B-3001 Leuven, Belgium*
[4]*Instituto de Astrofísica de Andalucía – SIC, Glorieta de la Astronomía s/n, E-18008 Granada, Spain*
[5]*Valencian International Univerisity, Prolongación C/José Pradas Gallen s/n, edificio B piso 2, E-12006 Castellón de la Plana, Spain*
[6]*Suhora Observatory and Krakow Pedagogical University, ul. Podchorążych 2, PL-30-084 Kraków, Poland*

Accepted 2014 February 28. Received 2014 February 28; in original form 2013 November 21

ABSTRACT

We analyse 2.75 yr of *Kepler* spacecraft observations of the pulsating subdwarf B star KIC 10670103. These 1.4 million measurements have an impressive duty cycle of 93.8 per cent, a frequency resolution of 0.017 μHz, and a 5σ detection limit of 0.1 parts-per-thousand (ppt). We detect 278 periodicities, making KIC 10670103 the richest pulsating subdwarf B star to date. Frequencies range from 23 to 673 μHz (0.4 and 11.8 h), with amplitudes from the detection limit up to 14 ppt. Follow-up spectroscopic data were obtained from which it was determined that KIC 10670103 does not show significant radial velocity variations. Updated atmospheric model fits determined $T_{\rm eff} = 21\,485 \pm 540$ K, $\log g = 5.14 \pm 0.05$, and $\log N({\rm He})/N({\rm H}) = -2.60 \pm 0.04$. We identify pulsation modes using asymptotic period spacings and frequency multiplets. The frequency multiplets indicate a spin period of 88 ± 8 d. Of the 278 periodicities detected in KIC 10670103, 163 (59 per cent) have been associated with low-degree ($\ell \leq 2$) pulsation modes, providing tight constraints for model fitting. While the data are exquisite, amplitudes (and some frequencies) are not stable over the course of the observations, requiring tools which are non-standard for compact pulsators such as sliding Fourier transforms and Lorentzian fitting. Using the 163 identified pulsation modes, it is possible to make detailed examinations of the pulsation structure; including where the pulsation power is concentrated in radial order, over what frequency range mode trapping is inefficient, and how power switches between multiplet members.

Key words: stars: oscillations – subdwarfs.

1 INTRODUCTION

Launched in 2009, the *Kepler* spacecraft's primary mission is to discover and characterize extrasolar planet transits. Success has been dramatic with over 2500 exoplanet candidates discovered so far. See Tenenbaum et al. (2013, and references therein) for discussions of these amazing results. For reviews of *Kepler* image processing and spacecraft data characteristics, see Jenkins et al. (2010).

The *Kepler* spacecraft has also had a huge impact on stellar research. It has discovered at least 2377 eclipsing binary stars from which bulk characteristics (e.g. mass, radius, luminosity, distance) can be determined[1] (Prsa et al. 2011; Matijevič et al. 2012). The most remarkable advances have been in understanding the interiors of stars using asteroseismology. Asteroseismology is the process by which stellar pulsations are used to discern the physical condition of stars. The process includes matching stellar models to observations, associating periodicities with pulsation modes, and examining where the models succeed and fail. Slight mismatches between observations and models can provide insights to new physics or add constraints to previously assumed conditions. Of particular note are the solar-like oscillators for which *Kepler* data produced detailed asteroseismic results, and from which the following were discerned:

★ E-mail: mreed@sdbv.missouristate.edu

[1] The Kepler Eclipsing Binary Catalog is located at keplerebs.villanova.edu

© 2014 The Authors
Published by Oxford University Press on behalf of the Royal Astronomical Society

Downloaded from http://mnras.oxfordjournals.org/ at Missouri State University on December 3, 2016

mass, core mass, radius, age, rotation, and core rotation (e.g. Bonaca et al. 2012; García 2013, among others).

Kepler has also yielded breakthroughs in subdwarf B (sdB) asteroseismology. sdB stars are extreme horizontal branch stars with masses $\approx 0.5\,M_\odot$, low-mass ($<10^{-2}\,M_\odot$) hydrogen atmospheres, and spectroscopic features dominated by strong, Stark-broadened Balmer absorption lines, indicating temperatures from roughly 20 000 to 40 000 K (Heber 1984; Saffer et al. 1994). They have somehow shed their outer layers near the tip of the red giant branch and are equivalent to the exposed core of a horizontal branch star. Evidence supporting this assertion includes the detection of similar gravity (*g*-)mode pulsation properties in a cooler blue horizontal branch star (Østensen et al. 2012) and in red clump solar-like pulsators (Beck et al. 2012). There are two classes of sdB pulsators, separated by pulsation period. The short-period pressure (*p*-)mode pulsators were discovered in 1996 (Kilkenny et al. 1997) and are designated V361 Hya stars. They have periods of a few minutes with amplitudes typically under 1 per cent of their mean brightness. The longer period *g*-mode pulsators were first published in 2003 (Green et al. 2003) and are classified as V1093 Her stars. These have periods of an hour or two with somewhat lower amplitudes. Several stars, particularly those observed with *Kepler's* accuracy, show pulsations of both varieties, making them hybrids. Generally, their pulsations are predominantly one type with only a few frequencies of the other class, the exception being Kepler Input Catalog (KIC) 9472174, which seems to have an abundance of both types (Østensen et al. 2010a).

Kepler's first-year survey phase discovered 15 sdB pulsators (Østensen et al. 2010b, 2011) with three additional pulsators discovered from Guest Observer programs, all in the open cluster NGC 6791 (Pablo, Kawaler & Green 2011; Reed et al. 2012). Of these, only two stars predominantly have *p*-mode pulsations; therefore, *Kepler* observations will be most useful for studying *g*-mode sdB pulsators. Important discoveries so far include evenly spaced *g*-mode periods (Reed et al. 2011) and frequency multiplets (Pablo et al. 2011, 2012; Baran 2012; Baran et al. 2012; Østensen et al. 2012; Telting et al. 2012), both of which can be used to identify pulsation modes. The frequency multiplets also provide rotation periods and these have been found to be on the order of tens of days (see Table 2). This includes stars in binaries, making them subsynchronous rotators (Pablo et al. 2011, 2012; Telting et al. 2012), contrary to common perceptions that short-period binaries are tidally locked. The even period spacings also provide a challenge to pulsation models, which predicted strong mode trapping breaking up evenly spaced periods (e.g. Charpinet et al. 2002). A possible solution has been sought in the form of increased diffusion (Hu et al. 2009; Miller Bertolami, Córsico & Althaus 2012), but so far no models have been able to produce period spacings as consistent as observed (see Reed et al. 2011, for a full discussion of sdB *g*-mode period spacings).

To date, four papers have been published of extended *Kepler* observations of sdB pulsators. Nine months of data were examined for KICs 11558725 (Telting et al. 2012) and 2697388 (Baran 2012), 15 months for KIC 10139564 (Baran et al. 2012), and 27 months for KICs 2991403, 2438324, and 11179657 (Baran & Winans 2012). For all these stars, multiplets and low-degree asymptotic period spacings were detected. These studies were able to correlate a high percentage of periodicities with low-degree ($\ell \leq 2$) modes, and found that sdB stars are slow rotators (tens of days; see Table 2). This paper is our first in a series to use multiple years of *Kepler* data to apply precision observational asteroseismic constraints to pulsating sdB stars.

1.1 Associating periodicities with pulsation modes

The goal of asteroseismology is to understand the properties (both bulk and internal) of stars. To do so, detailed models must be constrained by observations, typically $T_{\rm eff}$ and $\log g$ from spectroscopy as well as associating periodicities with pulsation modes. If features in the pulsation spectrum can be utilized (e.g. trapped modes), then further tools may be applied to constrain models (e.g. Degroote et al. 2010). Pulsation modes can be described by the three quantized numbers, n, ℓ, and m, where n is the radial nodes between centre and surface, ℓ is the number of nodes on the surface, and m represents the surface nodes which pass through the pulsation axis. The papers described in the previous paragraph show how useful *Kepler* data are for identifying ℓ and m modes and describe the two chief methods used for pulsating sdB stars: frequency multiplets and period spacings.

Frequency multiplets are caused by rotation removing the degeneracy of the azimuthal, m, index. From Ledoux (1951) it can be shown that

$$\Delta\nu = \Delta m \Omega \left(1 - C_{n,\ell}\right), \tag{1}$$

where $\Delta\nu$ represents the shift from the degenerate or $m = 0$ mode frequency, Ω is the frequency of stellar rotation, and $C_{n,\ell}$ is the Ledoux constant. The Ledoux constant is small for *p*-modes, but for higher order *g*-modes it depends on the degree, ℓ, according to

$$C_{n,\ell} \approx \frac{1}{\ell\,(\ell + 1)}. \tag{2}$$

The m index has $2\ell + 1$ values ranging from $-\ell$ to ℓ in integer steps; $\ell = 1$ modes appear as triplets, $\ell = 2$ modes as quintuplets, and so on, if all m components are observed. Since the pulsations are observed as hotter or cooler regions on the stellar surface, the amplitudes are sensitive to the angle at which they are viewed (Dziembowski 1977; Pesnell 1985). As such, it is possible they can be used to determine the inclination angle of the pulsation axis. In practice, however, such discrimination is difficult because the intrinsic amplitudes are not known a priori and seldom appear with consistent patterns which could be used for constraining the axis. In principle, frequency multiplets can be used to determine the ℓ *and* m values of the modes, the stellar rotation period, and the inclination angle of the pulsation geometry. As such, they are extremely useful for applying asteroseismology.

Even period spacings were an unexpected result from the *Kepler* observations. Stellar models anticipated that sdB stars consisted of two main components: an extremely dense core which contained nearly *all* the mass but only half the radius, and a tenuous atmosphere which contained very little mass, but provided half the radius. It was anticipated that the connection between these two pieces would create large mode trapping, effectively erasing the signature of period spacings (e.g. see the detailed paper of Charpinet et al. 2002). In the asymptotic limit ($n \gg \ell$), stellar pulsations appear as standard harmonic oscillators to which *g*-mode periods follow the relationship

$$\Pi_{\ell,n} = \frac{\Pi_o}{\sqrt{\ell\,(\ell + 1)}} n + \epsilon, \tag{3}$$

where Π_o and ϵ are constants with units of time representing the fundamental radial period and details of stellar structure, respectively (see Unno et al. 1979; Aerts, Christensen-Dalsgaard & Kurtz 2010, among others). The period spacing relationship between two consecutive overtones is

$$\Delta\Pi_\ell = \frac{\Pi_o}{\sqrt{\ell\,(\ell + 1)}}, \tag{4}$$

Downloaded from http://mnras.oxfordjournals.org/ at Missouri State University on December 3, 2016

where $\Delta\Pi_\ell = \Pi_{\ell,n+1} - \Pi_{\ell,n}$. The relationships between $\ell = 1$ and 2 modes are

$$\Pi_{n,\ell=2} = \frac{\Pi_{n,\ell=1}}{\sqrt{3}} + C, \quad (5)$$

where C is a constant that is expected to be small and is zero if $\epsilon(\ell=2) = \epsilon(\ell=1)$ (as it was in Reed et al. 2011), and

$$\Delta\Pi_{\ell=2} = \frac{\Delta\Pi_{\ell=1}}{\sqrt{3}}. \quad (6)$$

From these relations, identifications of ℓ can be made, particularly for $\ell = 1$ and 2, which are the most commonly identified modes to date. At short periods, period spacings are not expected, as we are not in the asymptotic regime, while at extremely long periods, they are insensitive because of how closely they resemble small frequency differences (possibly including rotational multiplets). Even where period spacings seem to be prevalent, there are small deviations which should be interpretable, given sufficiently complete structural models. Attempts have already been made to more accurately model diffusion to prevent significant mode trapping (Hu et al. 2009; Miller Bertolami et al. 2012). Once mode trapping can be effectively damped in the models, its occurrence can be used to constrain internal structure, typically via chemical gradients.

In this paper, we report the analysis of 33 months of short cadence (SC) observations of KIC 10670103, the first sdB star to have period spacings detected (Reed et al. 2010). These were measured as 251.13 and 145.59 s for $\ell = 1$ and 2, respectively. From ∼30 d of survey-phase data, 27 g-mode frequencies were detected of which 26 were identified. Østensen et al. (2010b) measured $\log g = 5.11 \pm 0.04$ dex and $T_{\rm eff} = 20\,900 \pm 300$ K from spectroscopy obtained at the Nordic Optical Telescope, making KIC 10670103 the coolest sdB pulsator discovered to date.

2 DATA ANALYSIS

The *Kepler* spacecraft obtained exquisite data of high precision with nearly continuous coverage. *Kepler* obtains data in two modes: long cadence (LC), which obtains one integration about every 30 min, and SC, which obtains one integration every 58.85 s. Each cadence is actually a sum of 6.02 s exposures with 0.52 s of dead time. For details concerning *Kepler* data, see Gilliland et al. (2010). Since *Kepler* has limited memory storage, there are far fewer targets observed in SC than LC mode. For this analysis, we downloaded monthly SC data from the Mikulski Archive for Space Telescopes[2] as FITS files for Quarters 5 through 15. *Kepler* stopped observing at the beginning of Quarter 17 due to failures in two reaction wheels which govern pointing. Quarter 16 was recently released but is not included in our analysis as it would only have changed the resolution by 0.01 μHz and therefore not impacted the results. From the FITS files, we extracted barycentric times and raw fluxes. Monthly data sets were low-order spline fit to remove long-term (>1.5 d) trends, then normalized by the mean brightness. The fitting period was chosen to be comfortably longer than the period cut-off, beyond which pulsations should not be driven. Examinations of data using longer period fitting did not reveal any coherent variability, perhaps associated with a companion, and radial velocity (RV) measurements are consistent with that conclusion (see Section 2.2). The data were σ-clipped at 5σ, with σ calculated monthly, and finally the resultant modulation intensities ($\Delta I/I - 1$) were multiplied by 1000 so that Fourier amplitudes appear as parts-per-thousand (ppt; the same as millimodulation amplitudes). Sample light curves of 1 d of data near the beginning and end of the run are shown in Fig. 1.

From 33 months of SC data covering Quarters 5 (starting BJD 245 5276) through 15 (ending BJD 245 6304), and including nearly 1.4 million observations, the $1.5/T$ resolution is 0.017 μHz.[3] These data have a 93.8 per cent duty cycle, which include spacecraft safing events during Quarters 8 and 14. Fig. 2 shows the entire frequency spectrum [or Fourier transform (FT)] to just beyond the Nyquist frequency at 8495 μHz. The highest amplitude peaks are truncated, so that lower amplitude peaks can still be shown. The usual way to calculate the detection limit (Breger et al. 1994; Kuschnig et al. 1997) is four times the average value of the frequency spectrum (noted as 4σ) in a pulsation-free region (700–900 μHz would be a useful region in this case). However a 4σ limit would predict ≈89 spurious peaks above the detection threshold while a 5σ limit would predict ≈1. The 5σ detection limit was calculated to be 0.0975 ppt in the frequency spectrum and corresponds to a false-alarm probability of 0.55 (for 1.4 million independent frequencies).[4] As described in Section 2.1, actually fitting frequencies was a non-trivial exercise and as a result, no periodicities with amplitudes below 5σ were selected as intrinsic to the star.

KIC 10670103's pulsations are concentrated between 60 and 220 μHz (1.26 and 4.6 h; Fig. 2). Shortward of 50 μHz, the amplitudes appear to smoothly taper down, with the smallest detectable frequency near 23 μHz. Peaks below 10 μHz are attributed to systematics, most likely caused by uneven stitching of monthly data segments, which were not completely removed. Several known spacecraft artefacts appear in the high-frequency region; the highest frequency attributed to the star is at 673 μHz (25 min). Fig. 3 shows the window function for these data. The window function is a frequency spectrum of artificial, noise-free data of constant amplitude and phase sampled at the same times as the actual data. It represents noiseless data, but indicates where sampling-induced artefacts appear. The central peak of each panel is the input signal, so other peaks are artefacts, which will occur for any real peak in the data as well. The left-hand panel indicates that if frequencies closer than 0.05 μHz (231.48 d) have amplitudes <10 per cent of their neighbour's, they will be indistinguishable from artefacts. The right-hand panel indicates that aliases at the 3 and 2 per cent level occur 1.11 (10.43) and 1.65 μHz (7.01 d), respectively, from every peak in the data. The window function indicates that artefacts will only be an issue near the two high-amplitude peaks of $f113$ and $f115$ or if peaks are separated by less than 0.05 μHz.

2.1 Frequency detection

For ground-based or *Kepler's* survey-phase data, the analysis would proceed using peaks in the frequency spectrum to estimate frequencies and amplitudes, which would then be simultaneously fitted to the original light curve using a non-linear least-squares (NLLS) program and subsequently removed (pre-whitened) from the data by subtracting a sine function with properties of the fit. Examination of the pre-whitened FT would then be an indicator of the goodness-of-fit of the resultant NLLS solutions. Applying this process to 33

[2] http://archive.stsci.edu/kepler/

[3] Because of amplitude and/or phase variations, and interactions between frequencies, we list frequency errors in Table 1 as the Lorentzian fitting profile width and this may be a more accurate reflection of the frequency accuracy for any given peak.

[4] Using equation (13.8.7) of Press et al. (1992).

Downloaded from http://mnras.oxfordjournals.org/ at Missouri State University on December 3, 2016

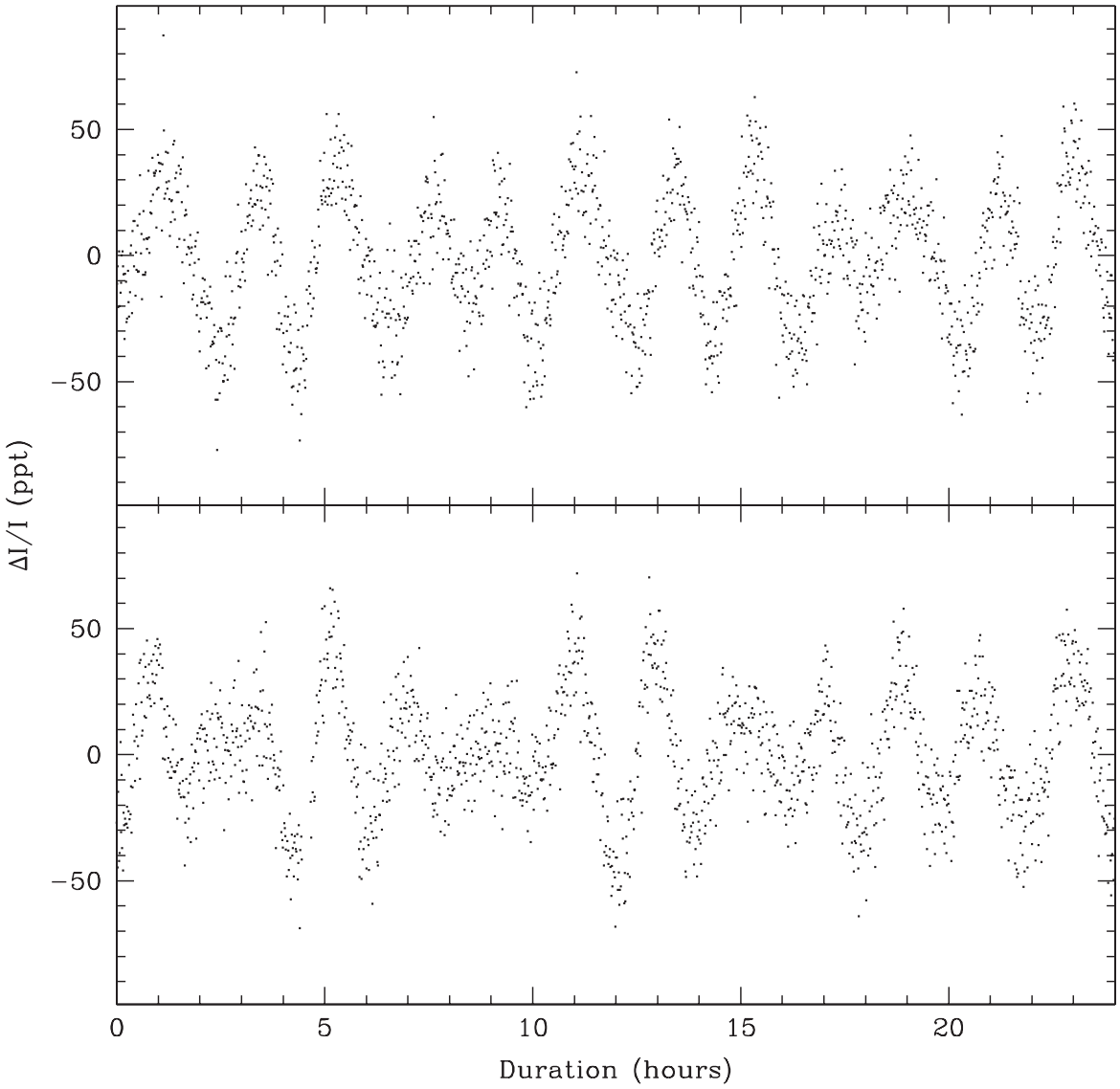

Figure 1. Sample light curves showing 24 h of data near the beginning (top) and end (bottom) of the run.

months of data met with little success; only 11 periodicities could be fit, but on the whole, their properties varied too much for NLLS fitting to work.

Long-term monitoring of sdB pulsators has indicated that they are not typically amplitude stable (e.g. Kilkenny et al. 2006; Reed et al. 2007), so we expected an NLLS analysis of the entire data set to be difficult. In general, the longer the observations, the more amplitude variability the data may contain and the more complex the analysis. The frequency spectrum shows the time-averaged value of any given peak and variability can generate artefacts which can be difficult to distinguish from real peaks (see Fig. 4). Pre-whitening would therefore remove the average amplitude, which would not represent the true signal within the data.

As such, we needed to apply different tools from what has become standard for pulsating sdB stars. An examination of the pulsation spectrum shows plenty of closely spaced frequency multiplets (see Fig. 6). These allow us to determine the minimum data length likely needed to resolve the pulsations. As frequency splittings were detected down to 0.06 μHz (see Section 2.1), a time span of 220 d (a frequency resolution of 0.05 μHz) was selected. Then sliding Fourier transforms (sFTs; Jacobsen & Lyons 2003) were produced to show how the pulsation spectrum changes during the observations. Selected regions of the sFTs are shown in Fig. 4 and were generated in the following manner: data were split into 220 d sets with 5 d steps. The first FT of the figures is centred 110 d after the time of the first data point and the next FT is centred 115 d after the first data point, and so on for each subsequent FT. So while the data began in Quarter 5, the *centre* of the first FT occurs in Quarter 6. Shown beneath each of the sFTs is the FT of the entire data set for that region. Fig. 4 clearly shows that the pulsation amplitudes changed over time. This figure shows select regions for discussion in Section 3.1, yet are reasonably representative of any region of the pulsation spectrum which contains pulsation power. (sFTs of all regions containing pulsations are included as supporting information.)

While the amplitude variations are obvious in Fig. 4, some frequency variations are evident as well. To determine if this is caused by resolution, we produced window sFTs for comparison, shown in Fig. 5. In all cases, the frequencies and amplitudes are fixed over the duration and indicate that what appear as frequency variations are

Downloaded from http://mnras.oxfordjournals.org/ at Missouri State University on December 3, 2016

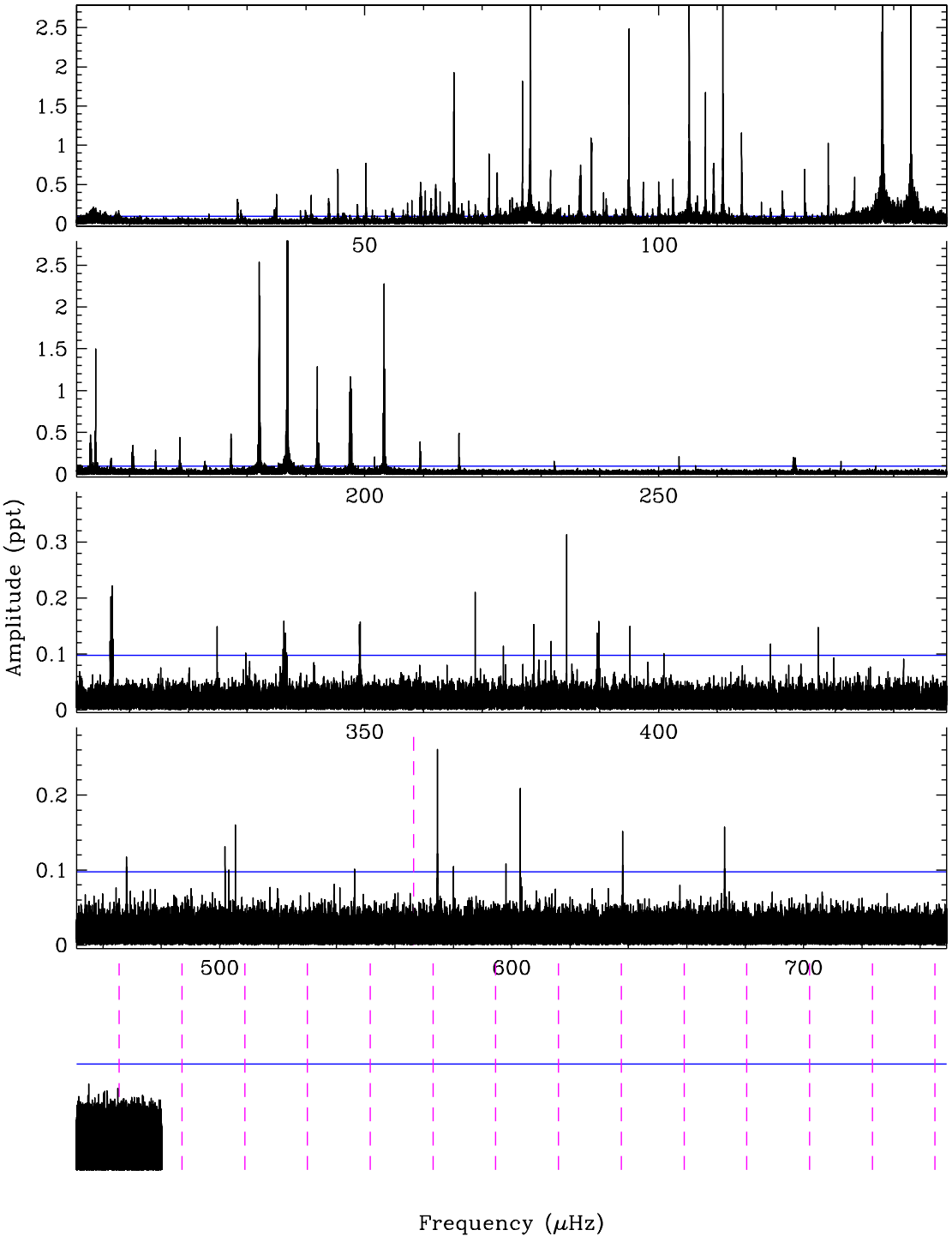

Figure 2. Temporal spectrum of the complete 33-month data set. The bottom two panels are at a different scale, as are the ordinates. The peaks at 78, 106, 112, 138, 143, and 187 μHz are truncated for clarity. Horizontal (blue) lines indicate the 5σ detection limit and dashed (magenta) vertical lines indicate known spacecraft artefacts.

caused by beating between the frequencies and are not intrinsic to the star. In comparing the *Kepler* sFTs to the window sFTs, we can conclude that the vast majority of the periodicities in KIC 10670103 are frequency stable (there are a few exceptions).

In order to estimate the frequencies and amplitudes of the periodicities, peaks in the frequency spectrum were fitted using a Lorentzian function. Lorentzian functions naturally fit Fourier spectra with non-constant (typically assumed to be decaying) amplitudes,[5] and we found the function provided a satisfactory fit (see Fig. 6). The Lorentzian linewidth was used as the estimated frequency error. While the frequencies can certainly be determined

[5] See http://www4.ncsu.edu/franzen/public_html/CH433/workshop/lineshape/ lineshape.html as an example and section 5.7 of Aerts et al. (2010).

Downloaded from http://mnras.oxfordjournals.org/ at Missouri State University on December 3, 2016

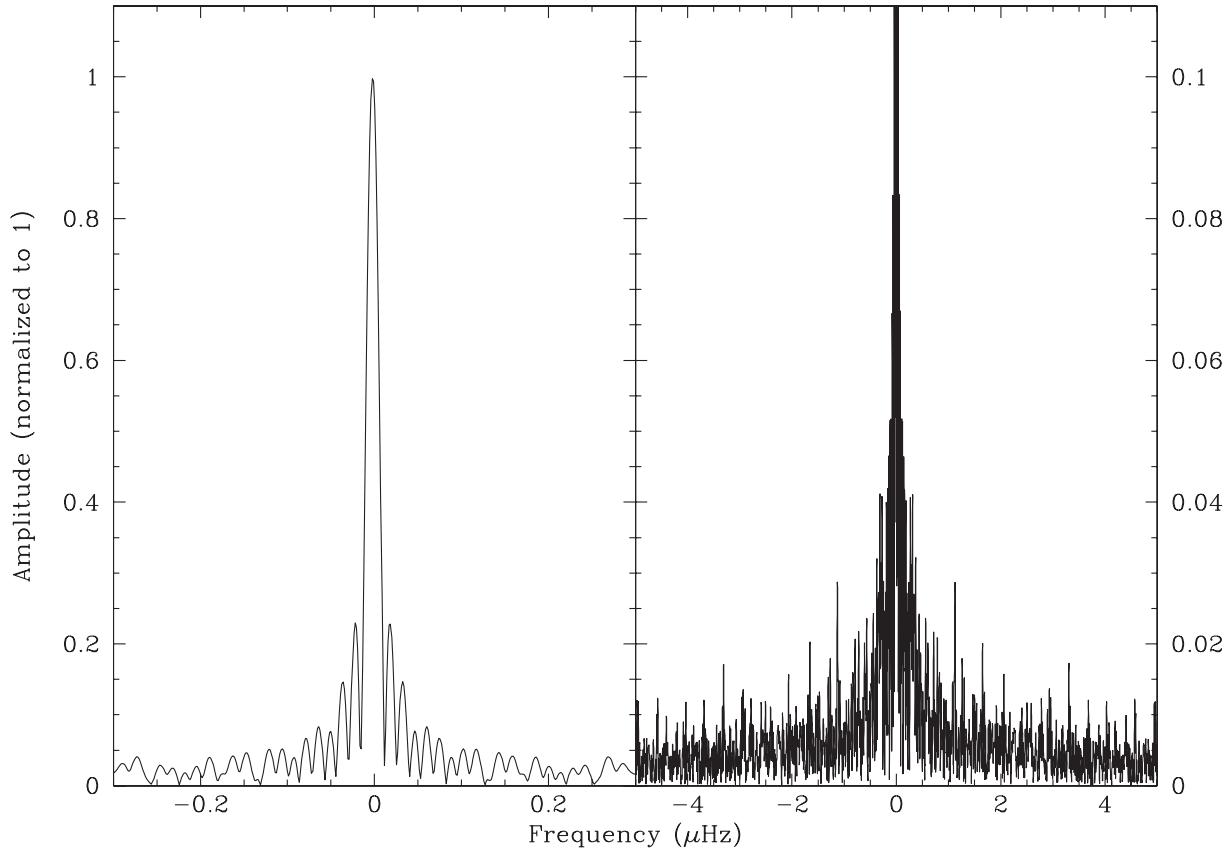

Figure 3. Window function shown at two different scales.

more accurately, the Lorentzian linewidth is a useful measure of the complexities contained within the data (i.e. changing amplitudes and/or phases). Any amplitude estimates can only be just that estimates. As is readily seen in the sFTs, the amplitudes in KIC 10670103 are constantly varying at some level, so the full FT only reflects median values and the peaks in the FT are distorted by amplitude variations (see Fig. 6). As such, the amplitudes listed in Table 1 are those from our Lorentzian fits of the entire data set; we estimate these to be accurate to about 0.03 ppt. All periodicities detected are listed in Table 1. Those recovered from Reed et al. (2011) are noted in column 15.

In total, 278 frequencies were fitted to the FT of all the data, except for f058 through f067, which were fitted to FTs only using data obtained towards the end of the observations. We provide the usual warning that while we used a 5σ detection threshold, periodicities which have amplitudes near the detection limit could be spurious and these should be considered tentative detections.

The frequencies are in a region estimated to be *g*-mode pulsations; the shortest period is near 25 min while the longest is nearly half a day. It is possible the shortest periodicities have a mixed *p*- and *g*-mode character, but a detailed model would be necessary to determine if such was the case, which is beyond the scope of this paper.

Some periodicities had so much variability in their amplitudes and/or phases and/or frequencies that complex structures appeared in the FT which could not reasonably be fitted. In these cases, we fitted Lorentzians to individual or groups of peaks as our 'best estimate', but by-and-large, we were only attempting to record that these regions have significant periodicities, even though we cannot necessarily determine the precise properties of the variability. These are noted in Table 1 and interested readers are encouraged to examine the sFTs (included as supporting information) or download the data from Mikulski Archive for Space Telescopes (MAST) to apply their preferred set of tools.

2.2 Spectroscopy

As part of our observing campaign to investigate the binary status of hot subdwarfs in the *Kepler* field (Silvotti et al. 2012; Telting et al. 2012), we obtained 30 low-resolution spectra of the Hη–Hβ region. Between 2010 July 28 and August 31, we obtained nine spectra with the Intermediate Dispersion Spectrograph and Imaging System (ISIS) on the William Herschel Telescope (WHT) with grating R600B and a 1.0-arcsec slit. On 2010 August 13 and 15, we obtained 11 spectra with the Kitt Peak 4-m Mayall telescope (KP4m) with RC-Spec/F3KB, the kpc-22b grating and a 2.0-arcsec slit. On the night of 2011 July 22, we obtained 10 spectra with the Andalucia Faint Object Spectrograph and Camera (ALFOSC) at the Nordic Optical Telescope (NOT), with grism #16 and a 0.5-arcsec slit.

Exposure times were typically 900 or 1200 s at the WHT. After rebinning to 0.7 Å pixel^{-1}, the median signal-to-noise ratio (S/N) of the spectra was 61, 36, and 34 for the WHT, KP4m, and NOT, respectively. The resulting resolutions based on the width of arc lines are 1.7 Å for the KP4m and WHT set-ups and 2.2 Å for the set-up at the NOT.

RVs were derived with the FXCOR package in IRAF. We used the Hγ, Hδ, H8, and H9 lines to determine the RVs and used the spectral model fit (see next section) as a template.

Downloaded from http://mnras.oxfordjournals.org/ at Missouri State University on December 3, 2016

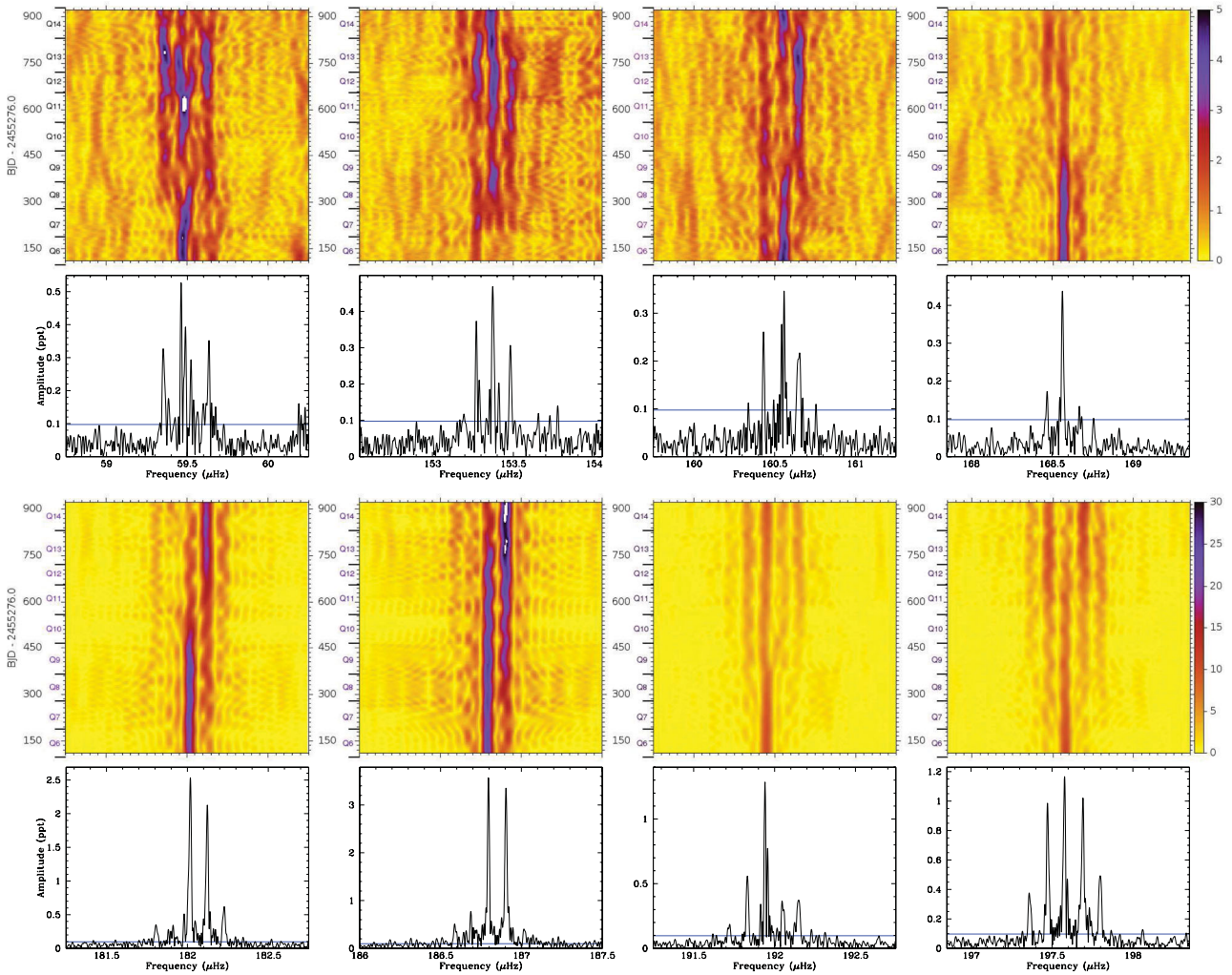

Figure 4. sFTs (top panels of each set) shown with FTs of the combined data set. Each line of the sFTs is a separate FT which spans 220 d and the ordinate indicates the mid-point of the data, which is why Quarters 5 and 15 do not appear, though those data are included in the sFTs. As such, quarter labels and separator bars on the ordinate indicate the *mid-point* of the data used in the individual FTs. Colour indicates amplitude in standard deviations (calculated as the average value of all constituent FTs) with a scale bar to the right of each panel). Bottom panels: FTs of the same regions from the entire data set. Horizontal (blue) lines indicate the 5σ detection limit. (Additional sFTs of other regions are available as Figures 13 to 17 in supporting information.)

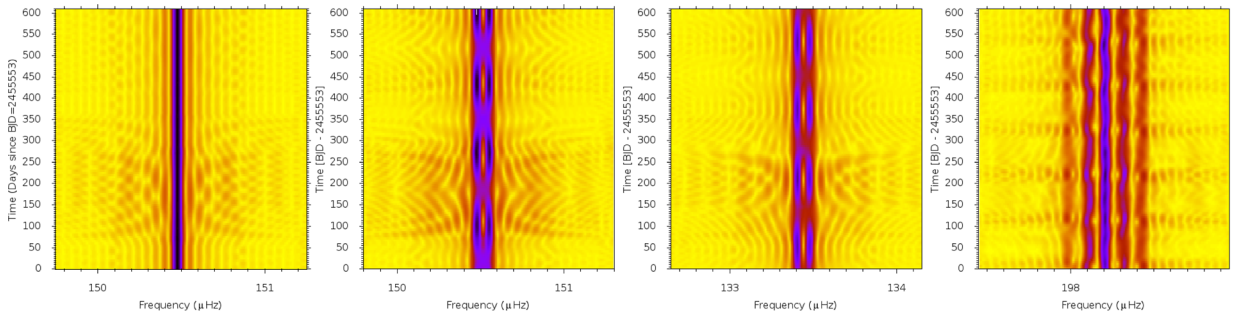

Figure 5. sFTs of window functions. From left to right: a single frequency; two same-amplitude frequencies separated by 0.69 μHz; using properties from Table 1 for a doublet ($f117$ and $f118$) and quintuplet ($f058$ through $f062$).

We found median values of the RV of $-28(3)$ km s^{-1}, $-30(3)$ km s^{-1} and $-40(3)$ km s^{-1}, for WHT, KP4m and NOT, respectively, with rms of 7, 7, and 8 km s^{-1}. The different median RV measured at NOT is probably a systematic instrumental offset. Within the errors of the individual measurements, we do not find any signal that hints at binarity. Gravity mode pulsation velocities are expected to be <1 km s^{-1} (e.g. For et al. 2006) which is well under what we could have detected.

As in Østensen et al. (2010b, 2011), we have fitted the average spectrum from each observatory to model grids, in order to determine effective temperature ($T_{\rm eff}$), surface gravity ($\log g$), and photospheric helium abundance ($\log y = \log N_{\rm He}/N_{\rm H}$). The fitting

Downloaded from http://mnras.oxfordjournals.org/ at Missouri State University on December 3, 2016

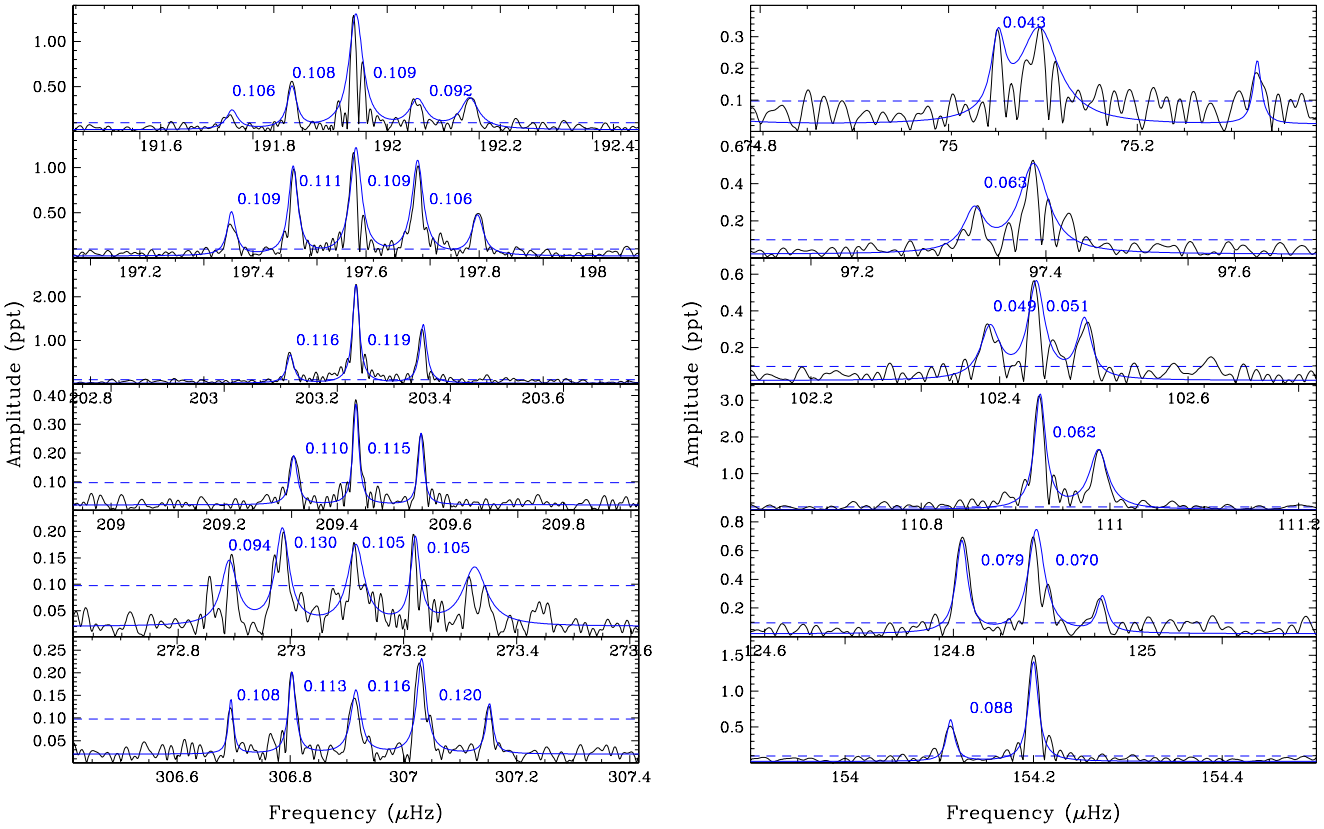

Figure 6. Examples of frequency multiplets. Left-hand panel: $\ell = 2$ multiplets with splittings of roughly 0.11 μHz. Right-hand panel: $\ell = 1$ multiplets with splittings of roughly 0.07 μHz. The horizontal dashed (blue) line is the 5σ detection limit.

Table 1. Pulsation properties and mode identifications. The frequency/period errors are the corresponding Lorentzian linewidths. Columns 5, 6, and 7/8 provide our best estimate of the mode degree ℓ, the azimuthal order m, and the radial overtone n fit to $\Pi_{\ell,n} = \Pi_{\ell,n=0} + n\,\Delta\Pi_\ell$, where $\Pi_{\ell=1,n=0}$ was estimated to be close to the radial fundamental mode. Column 9 or 10 provides the fractional deviation from even period spacing, and column 11 lists the frequency splitting from the subsequent frequency, if it may be part of a multiplet. Columns 12, 13, and 14 indicate the mode degree ℓ based on frequency multiplets, the value of the Ledoux constant from the frequency splitting (assuming $\Delta m = 1$), and period spacing, respectively. The last column provides the frequency ID notation from Reed et al. (2010). (This is a sample table. Full table available as supporting information.)

ID	Frequency (μHz)	Period (s)	Amplitude (ppt)	ℓ	m	n_1	n_2	$\delta P/\Delta\Pi_1$	$\delta P/\Delta\Pi_2$	$\Delta\nu$ (μHz)	Mode ID method νM	$C_{n,\ell}$	PS	M10
f001	672.977 (17)	1485.93 (0.04)	0.16	–	–	–	–	–	–	–	–	–	–	
f002	637.986 (16)	1567.43 (0.04)	0.15	2	–	–	8	–	0.03	–	–	–	2	
f003	602.977 (16)	1658.44 (0.04)	0.21	–	–	–	–	–	–	–	–	–	–	
f004	598.084 (06)	1672.01 (0.02)	0.11	1	–	4	–	0.10	–	–	–	–	1	
f005	580.021 (23)	1724.08 (0.07)	0.10	2	–	4	9	0.10	0.11	–	–	–	1 or 2	
f006	574.573 (21)	1740.42 (0.06)	0.26	–	–	4	9	0.17	0.22	–	–	–	1 or 2	
f007	546.203 (26)	1830.82 (0.09)	0.10	2	–	–	10	–	0.16	–	–	–	2	
f008	505.333 (10)	1978.89 (0.04)	0.16	1	–	5	–	0.11	–	–	–	–	1	
f009	503.121 (06)	1987.59 (0.02)	0.10	–	–	–	–	–	–	–	–	–	–	
⋮	⋮	⋮	⋮	⋮	⋮	⋮	⋮	⋮	⋮	⋮	⋮	⋮	⋮	

procedure used was the same as that of Edelmann et al. (2003), using the metal-line blanketed local thermodynamic equilibrium (LTE) models of solar composition described in Heber, Reid & Werner (2000). Mean values from these three fits were computed using the formal fitting errors as weights and systematics between observatories were then factored into the errors. The resultant measurements are $T_{\rm eff} = 21\,485 \pm 540$ K, $\log g = 5.14 \pm 0.05$, and $\log y = -2.60 \pm 0.04$.

3 MODE IDENTIFICATION

The advantage of a *Kepler* quality data set has revealed itself in an abundance of published mode identifications. Prior to *Kepler* data, period-matching between models and observations (called the *forward method*) was the only single-filter photometric method for identifying pulsation modes in sdB stars, and only for p-mode pulsators. Previous work on mode identification using *Kepler* data

Downloaded from http://mnras.oxfordjournals.org/ at Missouri State University on December 3, 2016

include Baran (2012), Baran et al. (2012), Pablo et al. (2011, 2012), and Reed et al. (2011); by-and-large we follow those examples. We searched for frequency multiplets, which provide the first-pass mode identifications. Then Kolmogorov–Smirnov (KS) tests, combined with series of identified frequency multiplets, were used to form period spacing sequences (discussed in Section 3.2).

3.1 Frequency multiplets

Fig. 6 shows several sets of multiplets in KIC 10670103. As described in Section 1.1, these multiplets can be used to associate periodicities with pulsation modes, ℓ and m. The most easily detected quintuplets (being the most likely $\ell = 2$ candidates) show a frequency splitting of $\approx$0.11 μHz. Splittings similar to this value were therefore used to search for other $\ell = 2$ multiplets, and these are listed in Table 1 in column 11 with m values estimated in column 6. Where multiplets do not form complete sequences, the $m = 0$ component is chosen as the highest peak from the possible $m = 0$ frequencies. In total, 23 frequency multiplets (79 periodicities) were designated as $\ell = 2$ modes. These provided an average $\ell = 2$ frequency splitting of 0.11 $\pm$ 0.01 μHz. Nearly all the triplets showed the same frequency splittings and were accordingly designated as $\ell = 2$ modes.

Several of the frequency splittings were too small to be $\ell = 2$ modes and few of these were in groupings larger than triplets, and were usually detected only as doublets. Most of these splittings were near 0.07 μHz, which is just where we expected to find $\ell = 1$ modes given the relationships in equations (1) and (2). These extremely small splittings create some ambiguities, even in such long time-base data. With a frequency resolution of 0.02 μHz, $\ell = 1$, $\Delta m = 2$ splittings can easily be confused with $\ell = 2$, $\Delta m = 1$ ones. To discriminate between these, we used period spacings and/or pulsation amplitudes, with the assumption that higher amplitudes are $\ell = 1$ modes which suffer less geometric cancellation. In total, 18 doublets and three triplets were designated as $\ell = 1$ modes, which are listed in columns 6 and 11 of Table 1 with six shown in the right-hand panel of Fig. 6. The 24 frequency splittings average to 0.07 $\pm$ 0.01 μHz.

Multiplets with more than five (including undetected) members are indicative of high-degree, $\ell \geq 3$, modes. In accordance with equation (2), these should have small Ledoux constants ($\leq$0.92), and since the $\ell = 2$ splittings are also small, higher degree multiplets would be extremely difficult to distinguish. Additionally, there are few inclinations where geometric cancellation for all m values are nearly equal. As such, full septuplets or nonuplets would not be expected, but rather triplets, quadruplets, and quintuplets with some spacings double the $\ell = 2$ value. We do not find any obvious $\ell \geq 3$ multiplets, though $f211$ through $f217$ form an octuplet with a missing member. However, this region is quite messy and the extremely small frequency splittings (0.039 μHz) make an $\ell \geq 3$ interpretation unlikely. The sFT vaguely has the appearance of three intertwined frequencies and so while we have fit seven frequencies in the overall FT, we interpret this as a frequency variable, $\ell = 1$ triplet and note it as such in Table 1. As such, we are left with many frequencies, some of which appear in multiplets, for which we cannot assign modes.

Equation (1) indicates that frequency multiplets place constraints on the spin period of the star. Assuming values for the Ledoux constants for $\ell = 1$ and 2 modes from equation (2), the spin period is calculated as 88 $\pm$ 8 d (88 $\pm$ 10 from $\ell = 2$ multiplets and 84 $\pm$ 12 using 1 multiplets). The long spin period makes KIC 10670103 similar to the other sdB pulsators for which *Kepler* has allowed us to measure frequency multiplets (Pablo et al. 2011, 2012; Baran 2012; Baran et al. 2012; Baran & Winans 2012; Østensen et al. 2012; Telting et al. 2012).

The inclination of the pulsation axis can be estimated using the multiplets. While they are not entirely consistent, and the amplitudes vary with time, the amplitudes of the central $\ell = 2$ multiplet frequencies tend to be the highest. This confines the inclination to be more polar than equatorial. Normalizing each multiplet to the amplitude of the designated $m = 0$ mode provides average multiplet amplitudes shown in Fig. 7. One set was calculated using only the quintuplets and another including the triplets (assuming the triplets are the $m = -1$, 0 and +1 components). Comparing to amplitudes calculated from a representative model, the inclination is between 15° and 40°. The 21 $\ell = 1$ multiplets are less consistent. Doublets are observed with splittings indicating both $\Delta m = 1$ and 2, which means that in some cases, we are only seeing the $|m| = 1$ modes while others have $m = 0$ combined with a single $|m| = 1$ mode. Additionally, many of the identified $\ell = 1$ modes only appear as single frequencies, which presumably is the $m = 0$ component. Except for the $\Delta m = 2$, these configurations slightly favour a more polar pulsation inclination. There are also some common amplitude features in some sFTs which could be related to a changing pulsation inclination angle. This will be discussed in Section 4.

3.2 Period spacings

The search for consistent period spacings (hereafter just called period spacings where the consistency of the spacings is implied) in KIC 10670103 began using two separate techniques. The first was to use a KS test of the periods in Table 1, and the second was to use the series of five quintuplets as the starting point for an $\ell = 2$ sequence.

The KS test is a non-parametric test that compares a sample distribution (the periods of Table 1) with a reference distribution (equation 4; Chakravarti, Laha & Roy 1967) and has proven useful with white dwarf and sdB pulsators (Kawaler 1988; Winget et al. 1991; Reed et al. 2011). If there are common spacings between periods, the KS test will produce a large negative value at the spacing. The top panel of Fig. 8 shows that the KS test indicates a significant number of periods spaced near to 250 and 145 s. These values match the $\ell = 1$ and 2 modes determined by Reed et al. (2011) for KIC 10670103. The peak near 145 s is broad and multiply peaked, which is caused by the large number of $\ell = 2$ multiplets, while the peak near 250 s is sharper, as the $\ell = 1$ modes are mostly singlets or doublets. Using the indicated values, differences in periods were calculated and those that matched the KS test were noted as possible fits to the period spacing sequences. One weakness to the KS test is that it only determines if there is common spacings between periods, but is insensitive to whether those spacings form a sequence or not.

The remaining panels of Fig. 8 show the impact on the KS test of removing the periods identified as $\ell = 1$ and/or 2 modes. In the second (third) panel, periodicities identified as $\ell = 1$ (2) are removed and the corresponding peak(s) and overtones are effectively *pre-whitened* out of the KS test. The bottom panel shows the remaining periods when all of the identified $\ell = 1$ and 2 periods are pre-whitened; no significant peaks remain.

The second method was to use the most obvious of the $\ell = 2$ multiplets to see if they form a sequence. The separations of the $\ell = 2$ multiplets between 4626 and 6671 s (150–216 μHz) average 146 $\pm$ 3 s, all of which are consecutive overtones. Radial indices were assigned to these spacings using a zero-point near 11 min (near to where the radial fundamental should be) and a linear

Downloaded from http://mnras.oxfordjournals.org/ at Missouri State University on December 3, 2016

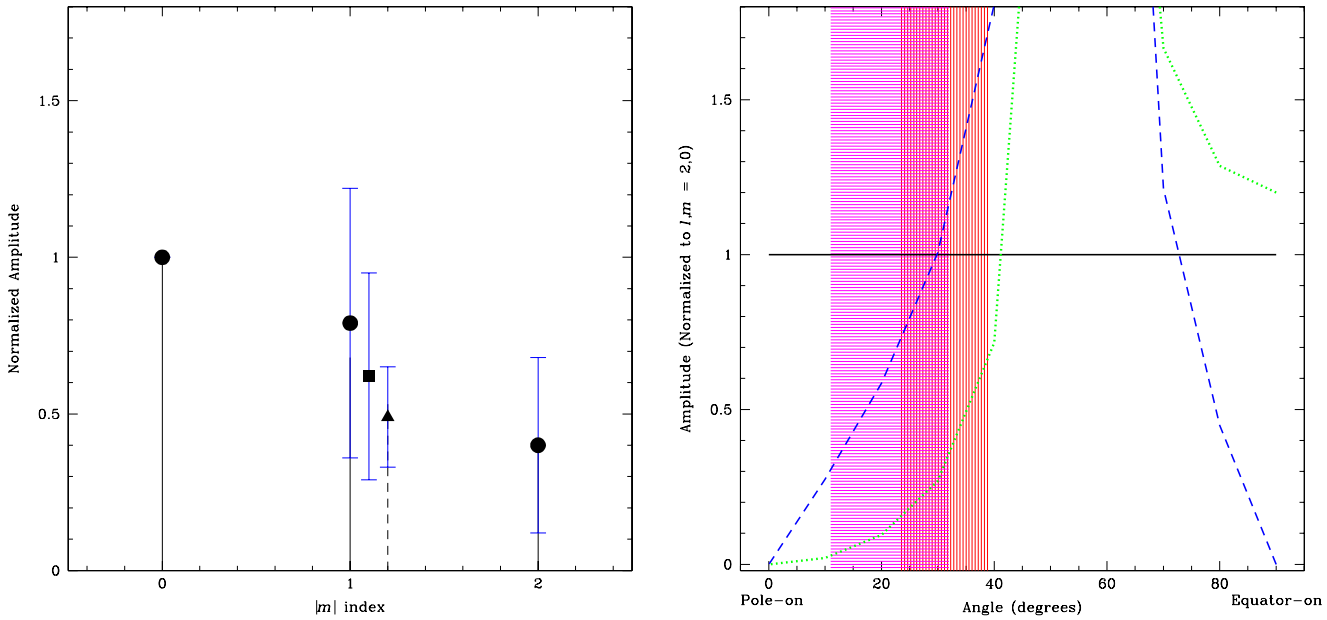

Figure 7. Pulsation axis inclination. Left-hand panel: average amplitudes of $\ell = 2$ multiplets normalized to ℓ, $m = 2, 0$. Circles are amplitudes from quintuplets only, triangles are using triplets only, and squares include both. Right-hand panel: model amplitudes (calculated in 10^0 increments) for all inclinations normalized to the ℓ, $m = 2, 0$ amplitude. Solid (black), dashed (blue), and dotted (green) lines are the $|m| = 0$, 1, and 2 modes, respectively. Shaded regions indicate inclinations which match the constraints from the left-hand panel. The shaded regions indicate the match between observations and a model for the $|m| = 1$ (horizontal and magenta) and $|m| = 2$ (vertical and red) modes for quintuplet error bars (circles in the left-hand panel).

regression was fit. From the linear regression, an $\ell = 2$ sequence was produced and periodicities which matched the sequence (within 10 per cent) were assigned as prospective $\ell = 2$ modes. Equation (5) was then used to produce an $\ell = 1$ model sequence from which periodicities were assigned as prospective $\ell = 1$ modes. This exercise was repeated using the $\ell = 1$ doublets with periods from 6495 to 16 850 s.

Period spacing sequences derived using the various methods were compared with the best results listed in Table 1. Typically, mode identifications were consistent between methods and so conflicts were few. Where the methods disagreed, first frequency multiplets and then deviations from the period sequence were used to determine which, if any, sequence a periodicity belonged to.

A final method of mode assignment is the use of an echelle diagram, as we have done in Fig. 9. These diagrams are visual representations of period spacings, but are useful as diagnostics of mode assignments. The diverging vertical lines indicate period separations caused by an $m = \pm 1$ frequency doublet ($m = \pm 2$ for the dashed blue lines in the left-hand panel). These lines indicate that period spacings as a mode identification method cease to be useful around 12 000 and 25 000 s for $\ell = 2$ and 1 modes, respectively. At these longer periods, the $m \neq 0$ modes will be sufficiently separated in period to generate confusion in the diagram. The size of the points indicates amplitudes, on a logarithmic scale for clarity. Since geometric cancellation increases with degree, low-degree modes should preferentially have higher amplitudes, unless offset by driving. This figure shows (as can also be determined from Table 1) that periodicities identified as $\ell = 1$ typically do have higher amplitudes than $\ell = 2$ modes. In cases where mode identification is ambiguous (i.e. the doublet at $f188/f189$), the amplitude can be used to infer the most likely mode.

As expected, the assigned $\ell = 2$ triplets and quintuplets line up nicely, with only a couple of exceptions. The exceptions are likely trapped $\ell = 2$ multiplets. Likewise, most of the doublets (black filled circles) line up as $\ell = 1$ modes with a few exceptions, which are likely trapped modes. The positioning of these trapped modes can be useful for indicating where steep density (or mean molecular weight) gradients occur (see Kawaler & Bradley 1994, for a discussion of mode trappings in white dwarf stars).

A linear regression solution of the most reliable period spacings resulted in $\Delta\Pi_{\ell=1} = 251.6 \pm 0.2$ and $\Delta\Pi_{\ell=2} = 145.0 \pm 0.1$, which are within the errors of the previous result (Reed et al. 2011). These relations, even determined independently via frequency multiplets, satisfy equation (6). 15 sets of periods satisfy equation (5) as having both $\ell = 1$ and 2 periodicities at the same radial overtone. If the periodicities are normalized by radial order using equation (3), it can be seen that KIC 10670103's pulsations are most unstable from $n \approx 29$ to ≈ 42. Comparisons with pulsation stability models could provide useful constraints, as it should be a measure of the cavity in which the instability occurs.

Column 4 of Table 1 provides our best-estimate mode identifications. Columns 11–13 provide mode identifications based on frequency multiplets, the value of the frequency splitting (which depends on the Ledoux constant only, assuming the star is spinning uniformly), and whether the period fits the period spacing sequences. The multiplet method is always a lower limit estimate, as it is possible that some multiplet members have amplitudes below the 5σ detection limit. The same is true for the frequency splittings of $\ell \geq 2$, as the Ledoux constant changes little, thus really only distinguishing $\ell = 1$ from $\ell \geq 2$ modes.

3.3 Unidentified periodicities

The next step is to assign modes to the unidentified periodicities. 115 periodicities are not identified as $\ell = 1$ or 2 modes and, other than $f017$–$f020$ and $f211$–$f217$, there are no multiplets detected beyond quintuplets, so that method is off-limits for KIC 10670103.

Downloaded from http://mnras.oxfordjournals.org/ at Missouri State University on December 3, 2016

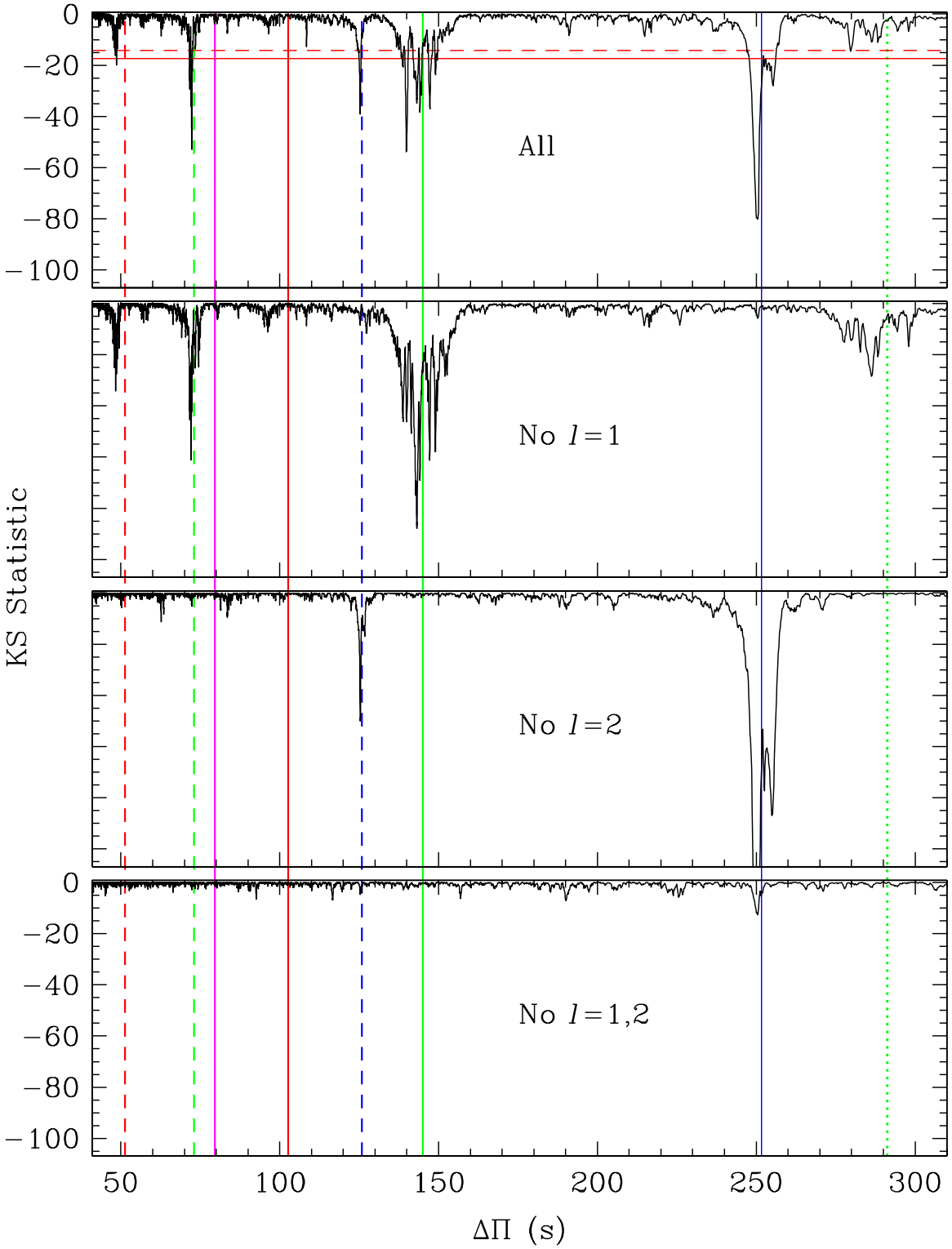

Figure 8. KS results for KIC 10670103. The top panel includes all of the periods of Table 1, while subsequent panels have the $\ell = 1$, 2, and 1 and 2 modes removed, respectively. The solid (dashed) horizontal line in the top panel indicates a 99 (95) per cent confidence level.

However, the KS test can be used as a diagnostic to search for $\ell \geq 3$ periodicities which obey equation (4). Once the $\ell = 1$ and 2 periodicities are pre-whitened out of the KS list, the result can be searched for peaks indicative of $\ell \geq 3$ spacings. This is shown in the bottom panel of Fig. 8. *If* the remaining periodicities are $\ell \geq 3$ *and if* they also follow the period spacing relations (i.e. are not trapped modes), then they should generate peaks according to equation (3). As evident in the figure, no such peaks exist. This indicates that *if* $\ell \geq 3$ modes are excited, they are not obeying the asymptotic period spacing relations.

Downloaded from http://mnras.oxfordjournals.org/ at Missouri State University on December 3, 2016

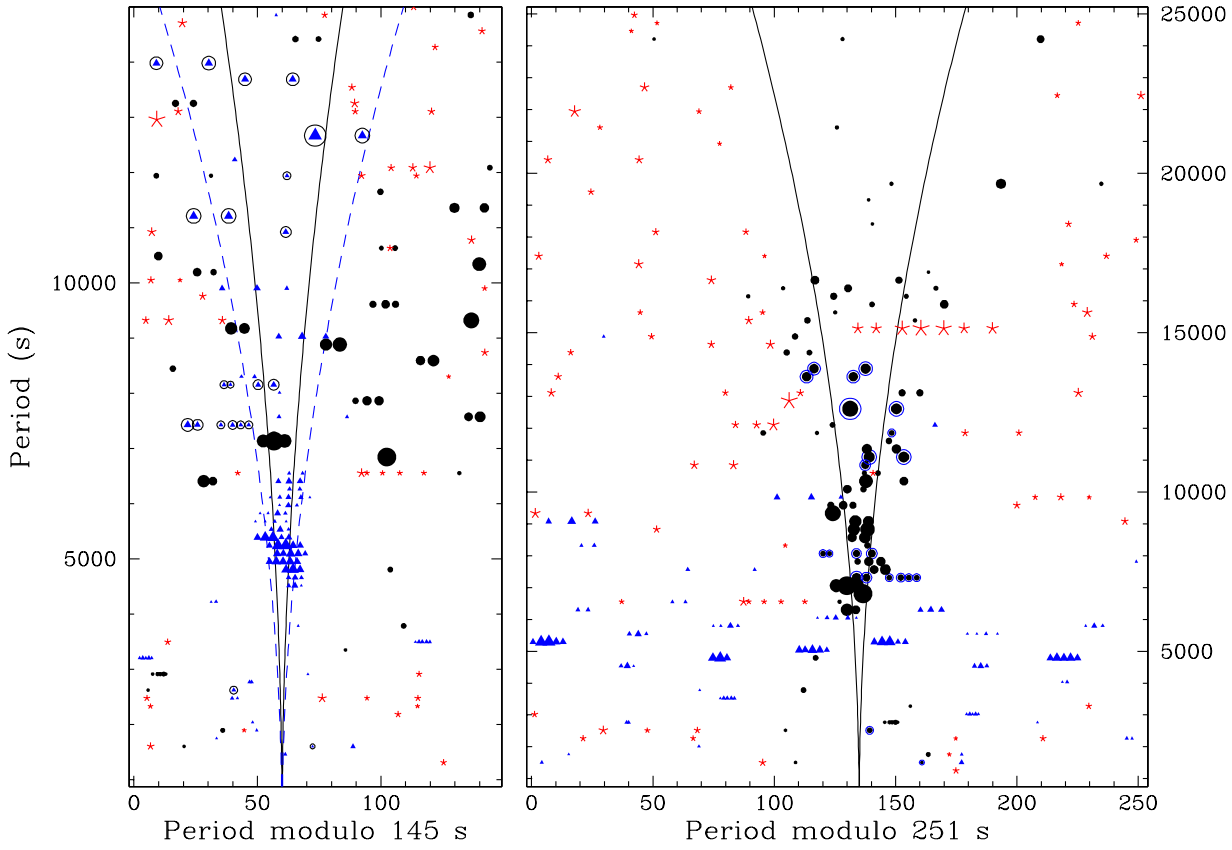

Figure 9. Echelle diagrams appropriate for $\ell = 2$ (left) and 1 (right) modes. Periodicities identified as $\ell = 1$ are shown as black circles, those as $\ell = 2$ are shown as blue triangles, and unidentified modes are red stars. Those which could be either $\ell = 1$ or 2 have circles around them. Size of the points indicates amplitude (logarithmic scale). Solid vertical lines indicate the distance between $m = \pm 1$ modes, and the dashed (blue) lines in the left-hand panel indicate $m = \pm 2$ modes. Ordinates are scaled so the longest period is that deemed detectable using period spacing. (This same figure with points colour coded by multiplet is available as Figure 12 in supporting information.)

4 SUMMARY AND CONCLUSIONS

From 33 months of nearly continuous *Kepler* data, we have detected 278 periodicities in KIC 10670103, making it the richest sdBV star observed, so far. The 93.8 per cent duty cycle provided excellent data with a 5σ detection limit of 0.1 ppt and a resolution of 0.017 μHz. We were able to associate 59 per cent of the periodicities with $\ell = 1$ or 2 modes using frequency multiplets and/or period spacings. From frequency multiplets, both ℓ and m were determined, and from period spacing, we could constrain ℓ and (relative) n. In addition to the straightforward splittings or spacings, the frequency splittings themselves provide a constraint on the Ledoux constant, $C_{n\ell}$. Since the Ledoux constant is mode dependent for g-modes, $C_{n\ell}$ can also be used to determine ℓ. Columns 12 through 14 of Table 1 provide mode identifications based on frequency multiplets (νM), values of the Ledoux constant ($C_{n\ell}$), and period spacings (PS).

4.1 Precision asteroseismology

Pulsation models have predicted various 'regions' of radial orders, which are unstable to pulsations (Charpinet et al. 2002; Jeffery & Saio 2006, 2007; Hu et al. 2009) depending on structure, composition, and which iron-bump elements are included in the stability calculations. These can now be directly compared to observations, recalling from equation (3) that periods (or frequencies) of the same radial order scale with ℓ. While the radial orders we have assigned have a somewhat arbitrary zero-point (we have chosen values to correspond roughly to where the radial fundamental periodicity should be), Fig. 10 aligns our identified modes with radial order. If we make the assumption that observable amplitudes indicate that the star is exciting those modes and not the modes which we do not detect, we can compare observed excitations with those from models. This can be taken a step further; if it is assumed that *all* azimuthal (m) orders are intrinsically excited, but the quantity detected is indicative of the excitation power (i.e. $\ell = 2$ modes which are driven with the most power are detected as complete quintuplets, those driven with less power are detected as triplets, and so on), we can determine where the pulsation power is concentrated in radial order. For the $\ell = 2$ modes, this occurs between $n = 29$ and 43, which is an uninterrupted sequence of multiplets containing all the quintuplets and all, save one, of the triplets. The $\ell = 1$ modes are more spread out, but multiplets are centred approximately in the same region as the $\ell = 2$ ones, including the majority of the triplets. Likewise, the echelle diagram can be modified to show only the identified modes for each panel over a fixed length of radial orders. This is shown in Fig. 11 and has some notable features. Even though there are $\ell = 2$ identified multiplets below $n = 30$, there is a 'turn-on' where period spacings begin and, roughly, a 'turn-off' around $n = 45$, after which there is a large gap and then only a few identified modes. The case is similar for $\ell = 1$, and the sequence extends further. For $24 \leq n \leq 48$, there is a nice sequence, above which, while there are identified $\ell = 1$ modes, the pattern is not nearly as well defined (using the

Downloaded from http://mnras.oxfordjournals.org/ at Missouri State University on December 3, 2016

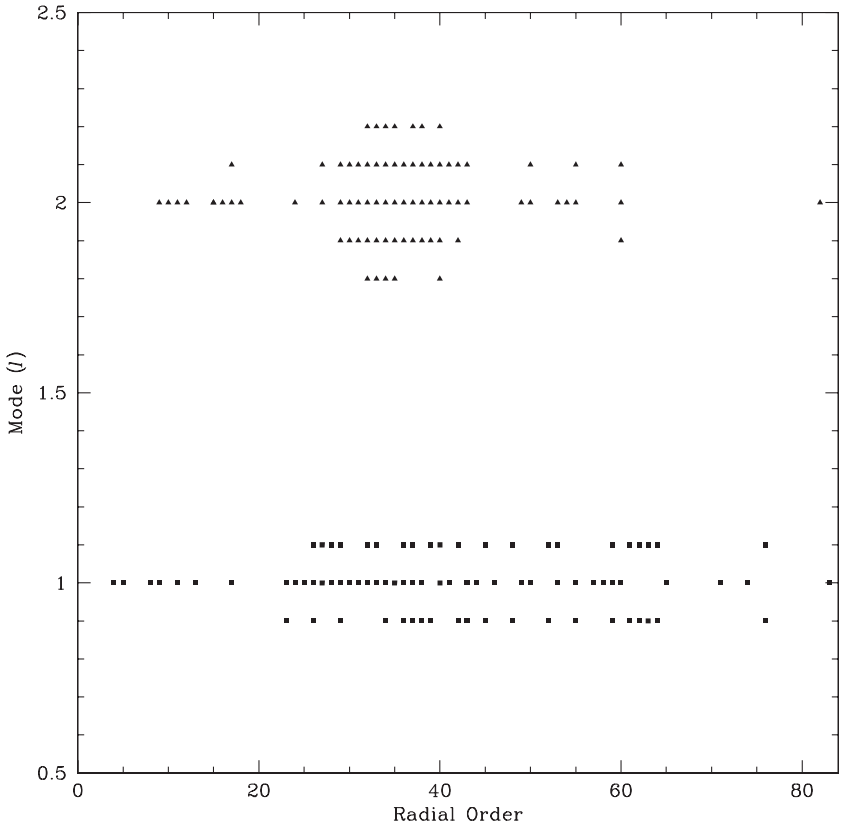

Figure 10. Comparison of excited modes and multiplets with radial order. Non-zero azimuthal orders are offset by 0.1 to indicate multiplets. Singlets are assumed to be $m = 0$ modes.

vertical lines as a guide). At the low-order side, it is most likely that the order is too low for the asymptotic approximation to be appropriate, and accordingly we have not identified singe frequencies as modes, even if they fit the period spacing sequence.

In particular, we would like to point out the $\ell = 2$ sequence from $f048$ through $f106$. This is an uninterrupted sequence of 15 *consecutive* overtones. Of the 59 frequencies in this region, only four do not belong to the sequence; one is unidentified, three fit $\ell = 1$ period spacing and two of these make a doublet with a Ledoux constant consistent with $\ell = 1$ modes. As such, of the 59 frequencies, only one remains unidentified and only two are not parts of multiplets where the Ledoux constant provides additional mode identification. This is an extremely powerful detection which may require a moment to digest. It is *not* that in this region there are many multiplets and frequencies, a selection of which can be associated with the $\ell = 2$ period spacing sequence. It *is* the case of an *extended, virtually perfect* sequence of frequencies, without gaps or ambiguity, all identified as $\ell = 2$ modes. Their $m = 0$ components deviate from equation (3) by <8 per cent (12 s) with an average value of 3.7 per cent (5.4 s). We are aware that recent work with theoretical models aims to reproduce features detected in *Kepler*-observed sdB pulsators (Hu et al. 2009; Miller Bertolami et al. 2012; Charpinet et al. 2013), but we are unaware of any result which can produce the purity of sequence found in KIC 10670103 (though Charpinet et al. 2013, may be very close). The sequence of $\ell = 1$ modes from $n = 23$ through $n = 46$ (and practically through $n = 65$) also form a nearly complete sequence of overtones. It is only missing the $n = 37$ mode and there are appropriate frequencies, $f157$ through $f159$, in this region, but their frequency splittings are appropriate for an $\ell = 2$ multiplet. In addition, many of the modes are identified using period spacings only, as many are not in multiplets and 38 per cent of the frequencies in this region are not associated with either sequence. As such, it is less restrictive than the $\ell = 2$ sequence. We would be very interested to see pulsation stability calculations from the latest generation Montreal models (described in van Grootel et al. 2013) or MESA[6] models appropriate for KIC 10670103's spectroscopic constraints, to see how close they come to matching the observations in these key regions. It may be that KIC 10670103's cooler temperature is what produces such pure sequences.

Figs 10 and 11 indicate that both $\ell = 1$ and 2 modes are most unstable to pulsation for the same radial orders n. Equation (3) shows that if the same radial order is excited, the higher degree ℓ mode will have the shorter period (higher frequencies), which is our result. The $\ell = 2$ multiplets occur between about 3000 and 6700 s (150–330 μHz), while the $\ell = 1$ multiplets occur between about 6500 and 16 900 s (60–155 μHz). Figs 9–12 of Jeffery & Saio (2006) show this effect for the regions of unstable modes of different degrees ℓ. If the model tables of Charpinet et al. (2002) went to high radial order, perhaps they would indicate if 'pockets' of modes unstable to pulsation align with radial order or period.

Additionally, each sequence has some small curvature caused by small amounts of mode trapping, which may be caused by the H/He boundary and evolve as this boundary does (Charpinet, private communication). Models may not be sufficiently mature to fully exploit the detail provided in these diagnostics, but recent investigations have begun to take into account their features (Charpinet et al. 2013) and we would very much like to see a detailed model

[6] see http://mesa.sourceforge.net/#paper

Downloaded from http://mnras.oxfordjournals.org/ at Missouri State University on December 3, 2016

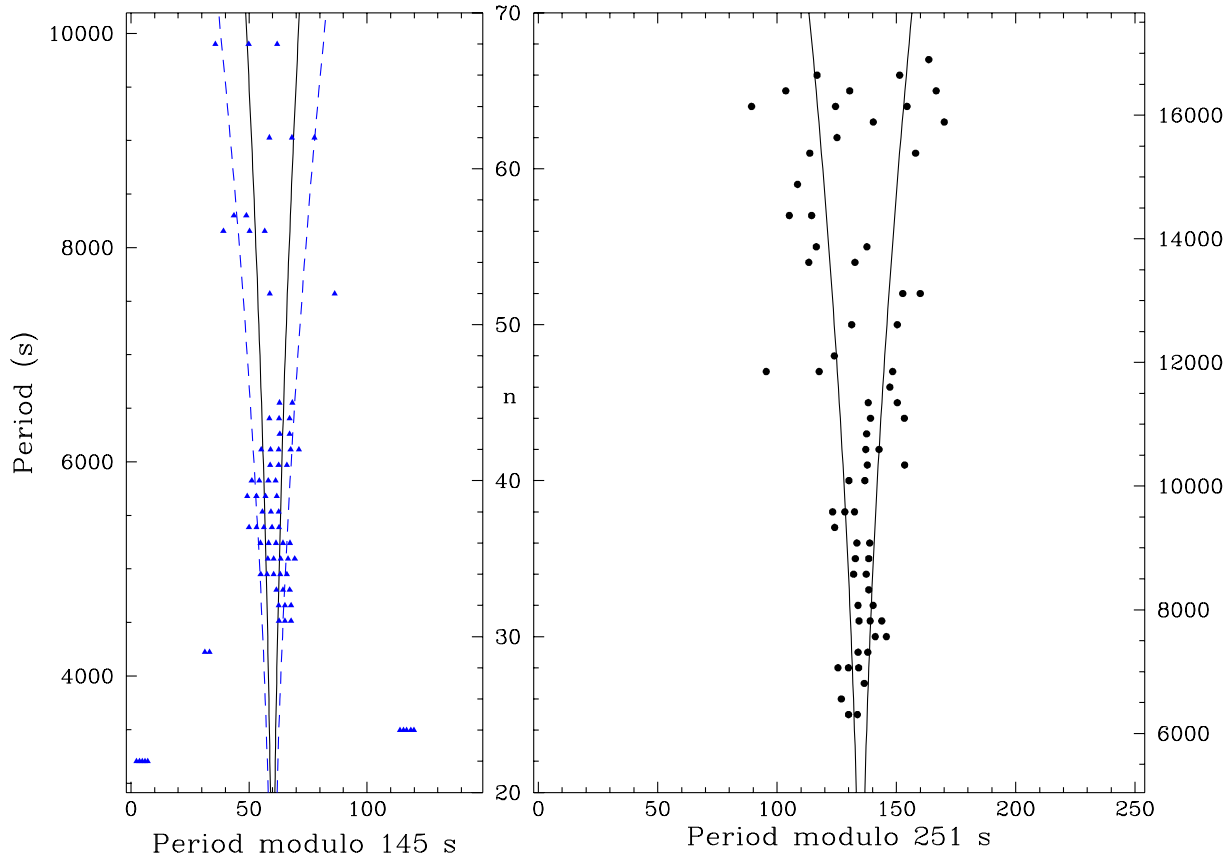

Figure 11. The same echelle diagrams as Fig. 9, except that *only* the identified modes for each appropriate panel are shown and the ordinate is scaled so the n indices match. The points are also uniform in size, rather than scaled with amplitude.

calculation which includes the features observed in KIC 10670103. We suspect that similar analyses on the other *Kepler*-observed stars may be useful for mapping out the driving regions and chemical features (i.e. boundaries) within sdB stars.

As shown in Fig. 4, some portions of multiplets appear to 'turn-on'; that is, their amplitudes become detectable during the course of the *Kepler* observations. Others appear to 'turn-off' and some do both. While some of the multiplets shown in Fig. 4 may give the impression that the central $m = 0$ component dominates early, with other components ramping up later, it is not consistent and many other multiplets have $m \neq 0$ components dominating early on, or a consistently low $m = 0$ component.[7] If there were a trend from the central component to the outer ones, then the most likely interpretation would be a precession of the pulsation axis. However, since it is not consistent, it most likely indicates that pulsation power is *switching* between the frequencies. Notice that the central component in the leftmost panel of Fig. 4, $f235$ goes from S/N of 5 to 1, and back to 5 in the span of ≈150 d. Similarly, the rightmost frequency of the rightmost panel, $f058$ goes from S/N of 1 to 3, and then continues to S/N of 6, each with about the same span of 150 d. However, the amplitude changes are complex and not consistent between different multiplets. While they indicate changes in pulsations, we do not have a way to interpret them within the context of current models to provide physical insight.

[7] See other examples in the supporting information.

4.2 Rotation properties

KIC 10670103 has a surprisingly long rotation period and has the coolest temperature for a pulsating sdB star, making it of particular interest. We also noted that the blue horizontal branch pulsator discovered by Østensen et al. (2012) also has an exceptionally long rotation period. While it is too early to read significance into it, Table 2 lists the rotation periods of hot horizontal branch pulsators organized roughly by position along the horizontal branch. Please note that three stars are in short-period binaries and are rotating subsynchronously. We include them for completeness but exclude them from consideration in the trend as their rotation periods are certainly being modified by their companions. Also included is the only ground-based example of multiplets observed in a non-binary star, Balloon 090100001. However, this last example is a p-mode-dominated hybrid pulsator, so it is somewhat exceptional to the g-mode sample. There is a marginal trend along the horizontal branch with longer rotation periods preferring the cooler/lower $\log g$ end. It will be interesting to see if this persists as long-term data allow multiplets to be discovered in other *Kepler*-observed sdB pulsators.

The current population does seem sufficient to conclude that sdB stars do not possess rapidly rotating cores, rotationally disconnected from the slowly rotating outer envelope as described in Kawaler & Hostler (2005) and Sills & Pinsonneault (2000). There must be a mechanism which effectively transports the core angular momentum to the envelope during either the ascent of the red giant branch, or the ensuing ejection of the envelope mass which produces the thin H atmospheres of sdB stars. The latter may be a more natural explanation which would incorporate the observed rotation velocity

Downloaded from http://mnras.oxfordjournals.org/ at Missouri State University on December 3, 2016

Table 2. Known rotation periods derived from multiplets.

Star ID	log g	$T_{\rm eff}$	$P_{\rm rot}$ (d)	Source
KIC 10670103	5.14 ± 0.05	$21\,485 \pm 540$	88 ± 8	This work
KIC 1718290	4.75 ± 0.03	$22\,350 \pm 200$	96.5	Østensen et al. (2012) and Østensen (2013)
KIC 2697388	5.32 ± 0.03	$23\,900 \pm 300$	45	Østensen et al. (2010b) and Baran (2012)
KIC 11179657[a]	5.14 ± 0.13	$26\,000 \pm 800$	7.2	Østensen et al. (2010b) and Baran et al. (2012)
KIC 2438324[a]	5.69 ± 0.10	$27\,098 \pm 823$	9.6	Pablo et al. (2011) and Baran et al. (2012)
KIC 2991403[a]	5.43 ± 0.03	$27\,300 \pm 200$	10.46	Østensen et al. (2010b) and Baran et al. (2012)
KIC 11558725[b]	5.41 ± 0.15	$27\,910 \pm 210$	45	Telting et al. (2012)
Balloon 090100001[c]	5.39	28 700	7.4	Telting & Østensen (2006) and Baran, Pigulski & O'Toole (2008)
KIC 10139564	5.67 ± 0.03	$31\,859 \pm 126$	25.6 ± 1.8	Baran et al. (2012)

[a]These stars are in binaries with periods ∼0.5 d.
[b]This star is in a 10 d binary.
[c]Ground-based observations.

break which occurs around 11 000 K (Recio-Blanco et al. 2004, and references therein) in horizontal branch stars. While such models are beyond the scope of this paper, we hope that *Kepler's* observational constraints will reinvigorate interest in solving this problem.

KIC 10670103 now represents another 'solved' sdB pulsator, joining the ranks of those listed in Table 2 and discussed in Section 1. The majority of periodicities have been associated with modes in these stars, typically $\ell = 1$ and 2, and many overtones have shown that mode trapping is minimal across several orders. What is lacking is theoretical interpretation. Prior to *Kepler* data, models were relatively unconstrained by observations, but this situation has quickly reversed, exposing weaknesses in the models. Some attempts have been made to update models to more appropriately match observations (Hu et al. 2009; Miller Bertolami et al. 2012; Charpinet et al. 2013), but a concerted theoretical effort is needed to interpret the precision of *Kepler's* data.

ACKNOWLEDGEMENTS

Funding for this Discovery mission is provided by NASA's Science Mission Directorate. The authors gratefully acknowledge the entire *Kepler* team, whose efforts have made these results possible. MDR also thanks Drs Tim Bedding and Dennis Stello for useful discussions about dealing with such amplitude-variable data. Funding for this research was provided by the National Science Foundation grants #1009436 and #1312869. Any opinions, findings, and conclusions or recommendations expressed in this material are those of the author(s) and do not necessarily reflect the views of the National Science Foundation. HF and LHF were supported by the Missouri Space Grant Consortium, funded by NASA. The research leading to these results has received funding from the European Research Council under the European Community's Seventh Framework Programme (FP7/2007–2013)/ERC grant agreement no 227224 (PROSPERITY) and from the Research Council of K. U. Leuven (GOA/2008/04).

The spectroscopic observations used in this work were obtained with the Mayall Telescope of Kitt Peak National Observatory, which is operated by the Association of Universities for Research in Astronomy under cooperative agreement with the National Science Foundation; the William Herschel Telescope located at the Observatorio del Roque de los Muchachos (ORM) and operated by the Isaac Newton Group; and the Nordic Optical Telescope also at the ORM and operated jointly by Denmark, Finland, Iceland, Norway, and Sweden. Some of the data presented in this paper were obtained from the Mikulski Archive for Space Telescopes (MAST). STScI is operated by the Association of Universities for Research in Astronomy, Inc., under NASA contract NAS5-26555. Support for MAST for non-HST data is provided by the NASA Office of Space Science via grant NNX13AC07G and by other grants and contracts. This paper includes data collected by the *Kepler* mission. Funding for the *Kepler* mission is provided by the NASA Science Mission directorate.

REFERENCES

Aerts C., Christensen-Dalsgaard J., Kurtz D. W., 2010, Asteroseismology, 1st edn. Springer Astronomy and Astrophysics Library, New York
Baran A. S., 2012, Acta Astron., 62, 179
Baran A. S., Winans A., 2012, Acta Astron., 62, 343
Baran A., Pigulski A., O'Toole S. J., 2008, MNRAS, 385, 255
Baran A. S. et al., 2012, MNRAS, 424, 2686
Beck P. et al., 2012, Nature, 481, 55
Bonaca A. et al., 2012, ApJ, 755, L12
Breger M. et al., 1994, A&A, 289, 162
Chakravarti I. M., Laha R. G., Roy J., 1967, Handbook of Methods of Applied Statistics. Wiley, New York
Charpinet S., Fontaine G., Brassard P., Dorman B., 2002, ApJS, 139, 487
Charpinet S., Brassard P., Van Grootel V., Fontaine G., 2013, in ASP Conf. Ser. Astron. Soc. Pac., San Francisco, in press
Degroote P. et al., 2010, Nature, 464, 259
Dziembowski W., 1977, Acta Astron., 27, 203
Edelmann H., Heber U., Hagen H.-J., Lemke M., Dreizler S., Napiwotzki R., Engels D., 2003, A&A, 400, 939
For B.-Q. et al., 2006, ApJ, 642, 1117
García R. A., 2013, Ap&SS, 31, 171
Gilliland R. L. et al., 2010, ApJ, 713, L160
Green E. M. et al., 2003, ApJ, 583, L31
Heber U., 1984, A&A, 130, 119
Heber U., Reid I. N., Werner K., 2000, A&A, 363, 198
Hu H., Nelemans G., Aerts C., Dupret M.-A., 2009, A&A, 508, 869
Jacobsen E., Lyons R., 2003, IEEE Signal Processing Magazine, 20, 74
Jeffery C. S., Saio H., 2006, MNRAS, 371, 659
Jeffery C. S., Saio H., 2007, MNRAS, 378, 379
Jenkins J. et al., 2010, ApJ, 713, L87
Kawaler S. D., 1988, in Christensen-Dalsgaard J., Frandsen S., eds, Proc. IAU Symp. 123, Advances in Helio- and Asteroseismology. Reidel, Dordrecht, p. 329
Kawaler S. D., Bradley P. A., 1994, ApJ, 427, 415
Kawaler S. D., Hostler S. R., 2005, ApJ, 621, 432
Kilkenny D., Koen C., O'Donoghue D., Stobie R. S., 1997, MNRAS, 285, 640
Kilkenny D., Kotze J. P., Jurua E., Brownstone M., Babiker H. A., 2006, Balt. Astron., 15, 255
Kuschnig R., Weiss W. W., Gruber R., Bely P. Y., Jenkner H., 1997, A&A, 328, 544

Downloaded from http://mnras.oxfordjournals.org/ at Missouri State University on December 3, 2016

Ledeoux P., 1951, ApJ, 114, 373
Matijevič G., Prša A., Orosz J. A., Welsh W. F., Bloemen S., Barckaly T., 2012, AJ, 143, 123
Miller Bertolami M. M., Córsico A. H., Althaus L. G., 2012, in Kilkenny D., Simon Jeffery C., Koen C., eds, ASP Conf. Ser. Vol. 452, Fifth Meeting on Hot Subdwarf Stars and Related Objects. Astron. Soc. Pac., San Francisco, p. 175
Østensen R. H., 2013, in ASP Conf. Ser. Astron. Soc. Pac., San Francisco, in press
Østensen R. et al., 2010a, MNRAS, 408, L51
Østensen R. et al., 2010b, MNRAS, 409, 1470
Østensen R. et al., 2011, MNRAS, 414, 2860
Østensen R. H. et al., 2012, ApJ, 753, L17
Pablo H., Kawaler S. D., Green E. M., 2011, ApJ, 740, L47
Pablo H. et al., 2012, MNRAS, 422, 1343
Pesnell W. D., 1985, ApJ, 292, 238
Press W. H., Flannery B. P., Teukolsky S. A., Vetterling W. T., 1992, Numerical Recipes in Fortran: The Art of Scientific Computing. Cambridge Univ. Press, New York
Prsa A. et al., 2011, AJ, 141, 83
Recio-Blanco A., Piotto G., Aparicio A., Renzini A., 2004, A&A, 417, 597
Reed M. D., Terndrup D. M., Zhou A.-Y., Unterborn C. T., An D., Eggen J. R., 2007, MNRAS, 378, 1049
Reed M. D. et al., 2010, MNRAS, 409, 1496
Reed M. D. et al., 2011, MNRAS, 414, 2885
Reed M. D., Baran A., Østensen R. H., Telting J., O'Toole S. J., 2012, MNRAS, 427, 1245
Saffer R. A., Bergeron P., Koester D., Liebert J., 1994, ApJ, 432, 351
Sills A., Pinsonneault M., 2000, ApJ, 540, 489
Silvotti R. et al., 2012, MNRAS, 424, 1752
Telting J. H., Østensen R. H., 2006, A&A, 450, 1149
Telting J. H. et al., 2012, A&A, 544, A1
Tenenbaum P. et al., 2013, ApJS, 206, 5
Unno W., Osaki Y., Ando H., Shibahashi H., 1979Nonradial Oscillations of Stars. University of Tokyo Press, Tokyo
Van Grootel V., Charpinet S., Brassard P., Fontaine G., Green E. M., 2013, A&A, 553, 97
Winget D. E. et al., 1991, ApJ, 378, 326

SUPPORTING INFORMATION

Additional Supporting Information may be found in the online version of this article:

Table 1. Pulsation properties and mode identifications.
Figures 13 to 17. Sliding FTs in 15 μHz segments.
Figure 12. Echelle diagrams appropriate for $\ell = 2$ and 1 modes.
(http://mnras.oxfordjournals.org/ lookup/suppl/doi:10.1093/mnras/stu412/-/DC1)

Please note: Oxford University Press is not responsible for the content or functionality of any supporting materials supplied by the authors. Any queries (other than missing material) should be directed to the corresponding author for the article.

This paper has been typeset from a TEX/LATEX file prepared by the author.

Downloaded from http://mnras.oxfordjournals.org/ at Missouri State University on December 3, 2016